Available online at www.sciencedirect.com
ScienceDirect
Acta Materialia 54 (2006) 4699–4707
Acta MATERIALIA
www.actamat-journals.com

Atomistic calculations of interfacial energies, nucleus shape and size of θ' precipitates in Al–Cu alloys

S.Y. Hu [a,*], M.I. Baskes [a], M. Stan [a], L.Q. Chen [b]

[a] *MST-8, Los Alamos National Laboratory, Los Alamos, NM 87545, USA*
[b] *Department of Materials Science and Engineering, Pennsylvania State University, PA 16802, USA*

Received 25 March 2006; received in revised form 24 May 2006; accepted 1 June 2006
Available online 30 August 2006

Abstract

θ' (Al_2Cu) is one of the primary strengthening precipitates in Al–Cu alloys. Although the precipitation sequence of various metastable phases in Al–Cu alloys is well known, fundamental information such as the shape and critical size of a homogeneous θ' nucleus is not available. In this work, we developed modified embedded-atom method potentials for Al–Cu alloys. The interfacial energies between a θ' precipitate and the Al matrix along experimentally observed orientations were calculated and compared with prior first-principles calculations. The critical sizes and nucleation barriers were obtained through both the classic theory for homogeneous nucleation and atomistic calculations. The results demonstrate that a plate-shaped nucleus with a semicoherent match between three face-centered cubic Al units and two θ' units along the edge of the plate is energetically favored.

Keywords: Molecular dynamics; θ' precipitate; Interfacial energy; Nucleation; Aluminum alloys

1. Introduction

A combination of low density and high strength makes aluminum alloys one of the primary materials used for automobile and aircraft applications, where a high strength-to-weight ratio is a major design consideration. The most significant contribution to the high strength of heat-treatable aluminum alloys is spatially distributed fine precipitates formed from a supersaturated solid solution that act as obstacles to moving dislocations. The famous precipitation sequence during heat treatment of an Al–Cu alloy with a small amount of copper, solid solution $\rightarrow$ GPI $\rightarrow$ GPII $\rightarrow \theta' \rightarrow \theta$, is the textbook example involving age hardening [1]. GPI is a monolayer of copper atoms on {100} planes of face-centered cubic (fcc) Al–Cu solid solution, while GPII consists of two or more {100} layers of copper atoms separated by three aluminum layers. θ' (Al_2Cu) has a tetragonally distorted fluorite (C1) structure, whereas θ has a C16 structure. First-principles calculations [2] show that the vibrational entropy stabilizes the θ phase above $T = 150$–200 C° over θ' while θ' is more stable at lower temperature due to its more negative formation enthalpy. Experimental results demonstrated that the plate-like θ' (Al_2Cu) precipitate is one of the primary strengthening phases in Al–Cu alloys. There have been extensive experimental and theoretical investigations on its growth kinetics, morphology and strengthening mechanisms [3–7]. However, due to its metastable nature, there is a lack of fundamental thermodynamic and structural information with regard to the metastable precipitates. It is still not clear what is the energetic barrier for the homogeneous nucleation of a θ' particle, and how applied stresses and defects affect the nucleation of precipitates. Addressing these questions requires accurate thermodynamic data such as chemical free energies of metastable phases, lattice mismatch between precipitates and matrix, the elastic constants and interfacial energies.

A direct experimental measurement of interfacial energy is difficult but there have been a number of attempts to

* Corresponding author.
E-mail address: syhu@lanl.gov (S.Y. Hu).

1359-6454/$30.00
doi:10.1016/j.actamat.2006.06.010

estimate indirectly the interfacial energies of θ' precipitates. For example, using precipitate evolution data during the coarsening stage, Boyd and Nicholson [8,9] estimated that the interfacial energies are about 1.5 and 21.5 J/m^2 for coherent and semicoherent interfaces, respectively. Aaronson et al. [10] ignored the misfit strain at the coherent interface and replaced the lattice misfit at the semicoherent interface with equivalent dislocations. They calculated the interfacial energy by including two energetic contributions. The first arises from the difference in chemical bonding across the interface, and the second arises from the presence of misfit strain and/or misfit dislocations at the interface. The calculated interface energies were about 0.03 and 0.35 J/m^2 for coherent and semicoherent interfaces, respectively. More recently, Wolverton et al. [2,11] determined the interfacial energies of θ' precipitates using first-principles calculations at $T = 0$ K. They assumed the interfacial configuration $m{:}n = 3{:}2$, i.e., three fcc Al unit cells match two θ' unit cells in the θ' thickness direction. The interfacial energies from first-principles calculations are 0.235 and 0.615 J/m^2 for coherent and semicoherent interfaces, respectively. It can be seen that quite large differences exist in interfacial energies obtained by different methods, but results from the first-principles calculations are expected to be the most reliable.

Molecular dynamics (MD) simulations using empirical potentials are commonly used to study structures and energies [12]. The embedded-atom method (EAM) based on the density functional theory was first proposed by Daw and Baskes [13]. The modified embedded-atom method (MEAM) [14] is similar to EAM but it includes angular forces that provide a better description of elements and/or phases in alloys with low symmetry. MEAM has been successfully applied to calculations of thermodynamic properties of perfect and defective bulk metals and alloys and predictions of phase stability in quantitative agreement with experiment [15–17]. The main purpose of the work reported in the present paper was to calculate the interfacial energies of θ' precipitates in Al–Cu alloys and to study the energetically favored configurations of critical nuclei. We developed MEAM potentials for Al–Cu alloys using experimental data and first-principles calculations. Using the MEAM potentials, the dependence of interfacial energies on the interfacial configuration was systematically investigated. The energetically favored θ' nucleus was predicted both theoretically and numerically.

2. MEAM potentials for Al–Cu alloys

In the present work, the Al–Al, Al–Cu and Cu–Cu interactions are described by MEAM potentials. A detailed description of MEAM potentials and fitting procedures of the potential parameters can be found elsewhere [14,18,19]. Here, we briefly review the formulism for the reader's convenience. In MEAM potentials, the total energy of a system is written as

$$E = \sum_i \left[F(\bar{\rho}_i) + \frac{1}{2} \sum_{j(\neq i)} \phi(R_{ij}) S_{ij} \right], \quad (i = 1, 2, \ldots, N) \tag{1}$$

where N is the total number of atoms in the system, $\phi(R_{ij})$ is the pair interaction energy between atoms i and j separated by a distance R_{ij} and S_{ij} is a screening function discussed below. $F(\bar{\rho}_i)$ is the embedding function; it is taken as $F(\bar{\rho}_i) = AE_c(\bar{\rho}_i)\ln(\bar{\rho}_i)$. $\bar{\rho}_i$ is the background electron density at site i, A is an adjustable parameter and E_c is the sublimation energy.

Unlike EAM, where the electron density is assumed to have spherical symmetry, MEAM assumes that the background electron density $\bar{\rho}_i$ at site i is composed of a spherically symmetric partial electron density $\rho_i^{(0)}$ and angular contributions $\rho_i^{(1)}$, $\rho_i^{(2)}$ and $\rho_i^{(3)}$. Each partial electron density term has the following form:

$$\begin{aligned}
(\rho_i^{(0)})^2 &= \left[\sum_{j(\neq i)} \rho_j^{a(0)}(R_{ij}) S_{ij} \right]^2 \\
(\rho_i^{(1)})^2 &= \sum_{\alpha} \left[\sum_{j(\neq i)} \frac{R_{ij}^{\alpha}}{R_{ij}} \rho_j^{a(1)}(R_{ij}) S_{ij} \right]^2 \\
(\rho_i^{(2)})^2 &= \sum_{\alpha,\beta} \left[\sum_{j(\neq i)} \frac{R_{ij}^{\alpha} R_{ij}^{\beta}}{R_{ij}^2} \rho_j^{a(2)}(R_{ij}) S_{ij} \right]^2 - \frac{1}{3} \left[\sum_{j(\neq i)} \rho_j^{a(2)}(R_{ij}) S_{ij} \right]^2 \\
(\rho_i^{(3)})^2 &= \sum_{\alpha,\beta,\gamma} \left[\sum_{j(\neq i)} \frac{R_{ij}^{\alpha} R_{ij}^{\beta} R_{ij}^{\gamma}}{R_{ij}^3} \rho_j^{a(3)}(R_{ij}) S_{ij} \right]^2 - \frac{3}{5} \sum_{\alpha} \left[\sum_{j(\neq i)} \frac{R_{ij}^{\alpha}}{R_{ij}} \rho_j^{a(3)}(R_{ij}) S_{ij} \right]^2
\end{aligned} \tag{2}$$

where $\rho_j^{a(h)}(R_{ij})$ represents the atomic electron density at site i from atom j. R_{ij}^{α} is the α component of the distance vectorR_{ij} (α, β, $\gamma = x$, y, z). The partial electron densities contribute to the background electron density as follows:

$$\bar{\rho}_i = \rho_i^{(0)} \sqrt{1 + \Gamma_i} \tag{3}$$

where

$$\Gamma_i = \sum_{h=1}^{3} t^{(h)} \left[\rho_i^{(h)} / \rho_i^{(0)} \right]^2 \tag{4}$$

Here, $t^{(h)}$ ($h = 1$, 2 and 3) are adjustable parameters. The atomic electron density is given as

$$\rho^{a(h)}(R) = \rho_0 \exp[-\beta^{(h)}(R/r_e - 1)] \tag{5}$$

where $\beta^{(h)}$ ($h = 0$, 1, 2 and 3) and ρ_0 are adjustable parameters and r_e is the nearest-neighbor distance in the equilibrium reference structure. For a single element system, ρ_0 may be taken as unity without loss a generality. For a binary system, only the ratio of ρ_0 for the two elements is part of the model.

In MEAM, no specific functional expression is given directly to the pair interaction $\phi(R)$. For a pure element, it can be derived from the universal equation of state at 0 K as a function of nearest-neighbor distance R [20]

$$E^u(R) = -E_c(1 + a^*)e^{-a^*} \tag{6}$$

where $E^u(R)$ is the universal function for a uniform expansion or contraction in the reference structure, E_c is the sublimation energy, and

$$a^* = \alpha(R/r_e - 1)$$

$$\alpha = (9B\Omega/E_c)^{1/2}$$

Here, B is the bulk modulus and Ω is the equilibrium atomic volume. If we only consider the first nearest-neighbor interactions, the energy per atom in the reference structure can be written as follows:

$$E^u(R) = F(\bar{\rho}^0(R)) + \frac{Z}{2}\phi(R) \tag{7}$$

where Z is the number of nearest-neighbor atoms and $\bar{\rho}^0(R)$ is the background density for the reference structure. The expression $\phi(R) = \phi_{ii}(R)$ of the pair interaction is obtained as

$$\phi_{ii}(R) = \frac{1}{Z}[E^u(R) - F(\bar{\rho}^0(R))] \tag{8}$$

If we choose a perfectly ordered binary intermetallic compound as the reference structure, the same method can be used to determine the pair potential between two different atoms. For example, in the B1 (NaCl-type) reference structure, the energy per atom can be described as

$$E^u(R) = \frac{1}{2}[F(\bar{\rho}_i^0(R)) + F(\bar{\rho}_j^0(R)) + Z\phi(R)] \tag{9}$$

and the pair potential $\phi(R) = \phi_{ij}(R)$ can be obtained as follows:

$$\phi_{ij}(R) = \frac{1}{Z}[2E^u(R) - F(\bar{\rho}_i^0(R)) - F(\bar{\rho}_j^0(R))] \tag{10}$$

Interactions beyond first nearest neighbors are modified by the screening function. The amount of screening of an atom k to the interaction between atoms i and j is determined using a simple geometrical construction. Imagine an ellipse passing through atoms i, k and j. Its x-axis is determined by the atoms i and j. Then, the ellipse is described by

$$x^2 + \frac{1}{C}y^2 = \left(\frac{1}{2}R_{ij}\right)^2 \tag{11}$$

where

$$C = \frac{2(X_{ik} + X_{kj}) - (X_{ik} - X_{kj})^2 - 1}{1 - (X_{ik} - X_{kj})^2} \tag{12}$$

where $X_{ik} = (R_{ik}/R_{ij})^2$ and $X_{kj} = (R_{kj}/R_{ij})^2$.

The basic idea for the screening is the following. Two values C_{max} and C_{min} are chosen to define two ellipses with different lengths of the y-axis. If an atom k is located outside the larger ellipse, it is assumed that the atom k does not affect the interaction between the atoms i and j. In this case, the screening factor is 1. If an atom k is located inside the smaller ellipse, then it is assumed that the atom k completely screens the interaction between atoms i and j, and the screening factor is zero. The screening factor changes continuously when atom k is located between these two ellipses. The screening factor is defined as a smooth function of C:

$$S_{ikj} = f_c\left[\frac{C - C_{min}}{C_{max} - C_{min}}\right] \tag{13}$$

The smooth cutoff function has the form

$$f_c(x) = \begin{cases} 1 & x \geqslant 1 \\ [1 - (1-x)^4]^2 & 0 > x < 1 \\ 0 & x \leqslant 0 \end{cases} \tag{14}$$

The resultant many-body screening function between atoms i and j is determined as the product of the screening factors due to all other neighbor atoms k:

$$S_{ij} = \prod_{k(\neq i,j)} S_{ikj} \tag{15}$$

To fit properties, the MEAM uses 13 potential parameters for each pure element (Al and Cu) and another 12 parameters for the pair potential (Al–Cu). In the present work, fcc is taken as the reference structure for Al and Cu and B1 is taken as the alloy reference structure. Experimental data [14,21] for lattice constants, vacancy formation energy and elastic constants for fcc Al and Cu are used to fit the Al–Al and Cu–Cu potential parameters. The potential parameters of Al–Cu are determined by lattice constants of θ and θ' phases, and an estimated formation energy (0.18 eV/atom) of the θ phase based on its experimental and first-principles results. All fitted parameters are listed in Tables 1 and 2. A comparison of calculated materials

Table 2
Values of the screening parameters C_{ikj} (1 refers to Al and 2 refers to Cu atoms)

C_{ikj}	ijk					
	111	112	212	121	221	222
C_{min}	1.30	0.00	0.00	0.50	0.00	1.30
C_{max}	2.30	2.80	2.80	2.80	2.80	2.30

Table 1
The MEAM parameters of Al–Al, Cu–Cu and Al–Cu

Phase	E_c (eV)	A	r_e (nm)	α	ρ_0	$\beta^{(0)}$	$\beta^{(1)}$	$\beta^{(2)}$	$\beta^{(3)}$	$t^{(1)}$	$t^{(2)}$	$t^{(3)}$
Al (fcc)	3.35	1.07	0.286	4.64	1.0	2.04	1.50	6.00	1.50	6.00	−2.30	8.01
Cu (fcc)	3.54	1.07	0.256	5.11	2.0	3.63	2.20	6.00	3.20	2.00	2.49	2.59
AlCu (B1)	3.69		0.246	10.95								

E_c is the cohesive energy, r_e is the nearest-neighbor distance and $\alpha^2 = 9\Omega B/E_c$, where Ω is the equilibrium atomic volume of the reference structure and B is the bulk modulus.

Table 3
Calculated and experimental lattice constants a and c (nm) and energies ΔH (eV/atom)

Phase	a		c		ΔH		
	MEAM	Expt. [21]	MEAM	Expt. [21]	MEAM	Expt.	First principles
Al	0.405	0.405*	–	–	−3.35*	−3.34 [22]	−3.50 to −3.98 [23]
Cu	0.362	0.362*	–	–	−3.54*	−3.54 [22]	−2.98 to −4.42 [24]
θ	0.595	0.606*	0.482	0.487*	−0.18	−0.14 to −0.25 [21]	−0.17 to −0.20* [2]
θ'	0.406	0.405*	0.577	0.581*	−0.21	–	−0.20 to −0.23 [2]

The values marked with an asterisk are used to determine the potential parameters. For the pure elements ΔH represents the formation energy from atoms (cohesive energy) while for the compounds ΔH represents the formation energy from the elements.

properties and those obtained from experiments [21,22] and first-principles calculations [2,23,24] are given in Table 3. Using a switching procedure [25] and temperature integration of enthalpy, the free energies of θ and θ' phases as a function of temperature are calculated at zero pressure. The results are shown in Fig. 1. They indicate that the formation energy of the θ' phase is smaller than that of θ phase at 0 K. However, vibrational entropy reverses their stability around $T = 260$ K, which agrees with the first-principles calculations and vibration entropy estimates [2]. The temperature dependence of the elastic constants of fcc Al and Cu is also predicted by the developed MEAM potentials as shown in Fig. 2, where the experimental elastic constants [26] are plotted using solid lines for a comparison. These results demonstrate that the Al–Cu MEAM potentials provide a very good description of the energetic and elastic properties of Al–Cu alloys.

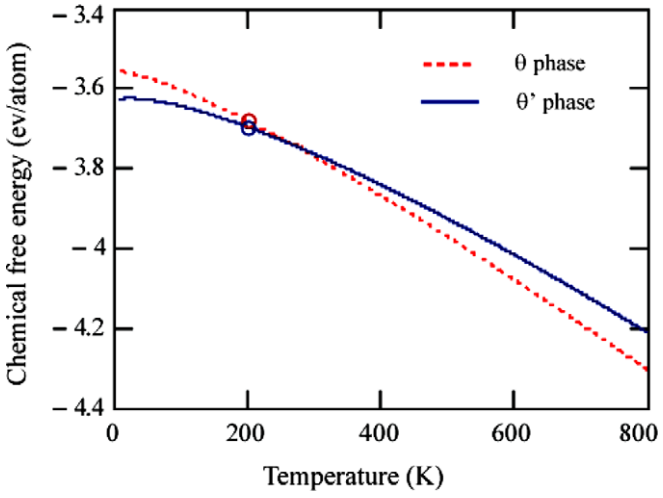

Fig. 1. Free energy of θ and θ' phases verses temperature. The symbols denote MD switching results while the curves represent the results of the temperature integration of the calculated average enthalpy.

3. Interfacial energies

θ' (Al_2Cu) has a tetragonal structure, as shown in Fig. 3. Experiments [7] demonstrated that θ' forms a plate-like precipitate in the matrix (fcc Al–Cu solid solution), which has a (001) broad interface and an orientation relationship $(001)_{\theta'}||(001)_{\text{matrix}}$ and $\langle 100\rangle_{\theta'}||\langle 100\rangle_{\text{matrix}}$. In addition, it is found that the broad interface of the plate-like θ' precipitate is coherent while the interface around the rim of the plate is semicoherent. Fig. 4 shows the θ' morphology obtained from transmission electron microscopy analysis. Because of different atomic structures and lattice constants between θ' and matrix along the thickness of the plate-like θ' precipitate, both the semicoherent interface configuration and its interfacial energy might depend on the semicoherent interfacial configuration, i.e., how many θ' and matrix unit cells match each other. It is not clear

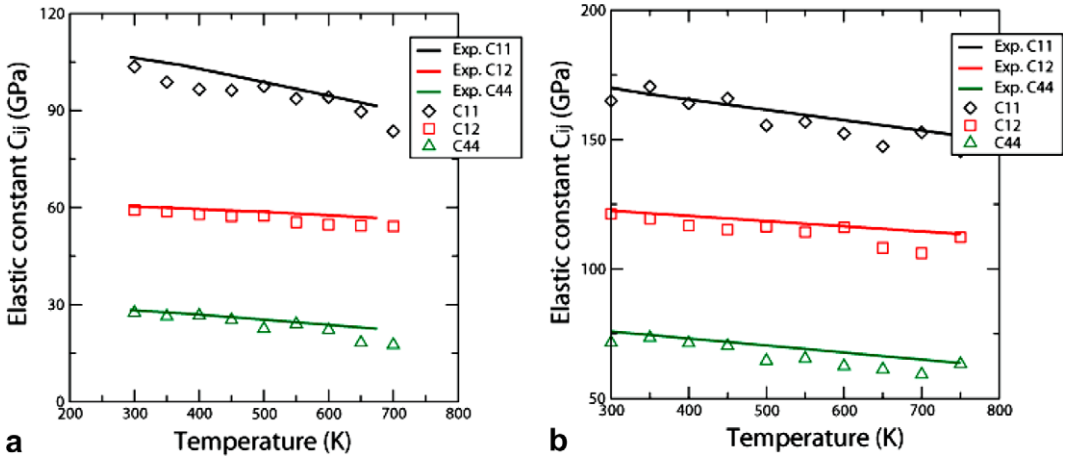

Fig. 2. Calculated (symbols) and experimental (lines) elastic constants as a function of temperature for (a) fcc Al and (b) fcc Cu.

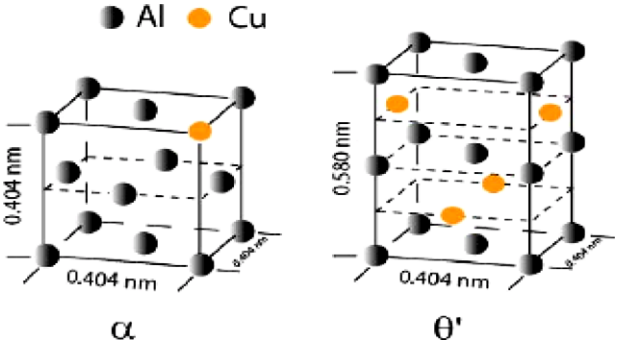

Fig. 3. Atomic structures of θ' and the fcc matrix.

what semicoherent interfacial configuration is energetically favored for θ' nucleation. The main purpose of this work is to calculate the interfacial energies of θ' precipitates in Al–Cu alloys and to study the energetically favored configuration of critical nuclei. Due to the fact that the θ' precipitate is a very thin, but large, plate (its thickness is usually a few nanometers and its diameter is about 100 nm), we can image that the lattice constants along [1 0 0] and [0 1 0] directions should be controlled by the lattice constant of the matrix while the stress along the [0 0 1] direction should be completely relaxed. To satisfy these constraints, periodic boundary conditions along the [1 0 0] and [0 1 0] directions and a stress-free condition in the [0 0 1] direction are applied for the calculations of coherent interfacial energies. Fig. 5(a) shows the simulation cell for the coherent interfacial energy calculations. Because of non-uniform deformation associated with the lattice mismatch along the θ' thickness direction, it is difficult to extract the interfacial energy from the total energy. Wolverton et al. [2] designed a method to subtract the elastic energy in their first-principles calculations. Their method, which is based on a uniform deformation assumption in both the θ' and matrix, is the correct method to calculate the interfacial energy if the θ' precipitate has an infinite thickness. As we know, θ' is a very thin plate. A deformation gradient exists across the semicoherent interface, which strongly depends on the interface configuration. Therefore, it is impossible to subtract completely the elastic energy. In this work, because the precipitate is thin, we simply assume that the precipitate thickness is constrained by the matrix, and assume that the stress along the [1 0 0] direction is completely relaxed in order to satisfy the equilibrium condition in the matrix just away from the interface region. In the calculations of semicoherent interfacial energies, periodic boundary conditions along the [0 1 0] and [0 0 1] directions and a stress-free boundary condition along the [1 0 0] direction are employed. Fig. 5(b) shows a simulation cell for the semicoherent interfacial energy calculations. The interfacial energy is calculated as

$$\gamma(m,n) = \frac{E(m,n) - E(m,Al) - E(n,\theta')}{2S} \tag{16}$$

where $E(m,n)$, $E(m,\mathrm{Al})$ and $E(n,\theta')$ are the total energies of atoms in the interface simulation cell, the part of pure Al and pure θ' under the same boundary conditions described above, respectively. S is the interface area.

In the simulations, we consider different semicoherent interface configurations m:n. The m, n and stress-free strain associated with the lattice mismatch are given in Table 4. Coherent and semicoherent interfacial energies versus stress-free strain are plotted in Figs. 6 and 7. As expected, the coherent interfacial energy is almost independent of the θ' thickness (stress-free strain). Checking the relaxed atomic structures, it is found that, although the θ' is initially deformed to fit the semicoherent interface configuration m:n, the θ' relaxes to its equilibrium lattice constant in the [0 0 1] direction. Since the lattice constants of θ' precipitates in the [1 0 0] and [0 1 0] directions are a little larger than that of the matrix, the θ' is subjected to a compressive stress which is about 0.42 GPa. The calculated coherent interfacial energy is 0.156 J/m^2, slightly smaller than the 0.235 J/m^2 obtained from first-principles calculations [2]. It should be pointed out that the first-principles calculations relax the whole simulation cell while our simulations assume that the lattice constants of the θ' precipitates in the [1 0 0] and [0 1 0] directions are fixed by the matrix. The compressive stresses in our simulations might reduce the coherent interfacial energy, as we have found that compressive stress reduces the (0 0 1) surface energy of the θ' phase. The semicoherent interfacial energies versus stress-free strains for different interface configurations m:n are plotted in Fig. 7. For the interface configuration m:$n = 3$:2 used in the first-principles calculations [2], the semicoherent interfacial energy is 0.694 J/m^2 while first-principles calculations give 0.615 J/m^2. As discussed above, the first-principles calculations and MD simulations employ different boundary conditions. Although the constraints used in MD and first-principles calculations do not reflect the experimental constraint, these calculations give a very close semicoherent

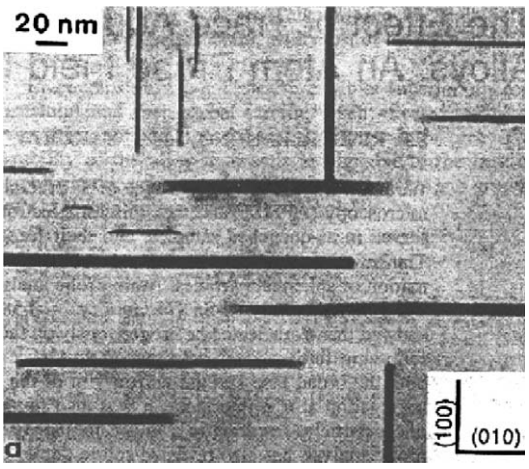

Fig. 4. Transmission electron micrograph of an Al-1.7 at.% Cu alloy aged at 190 °C for 30 h. The foils were oriented along [0 0 1] (from Ref. [26]).

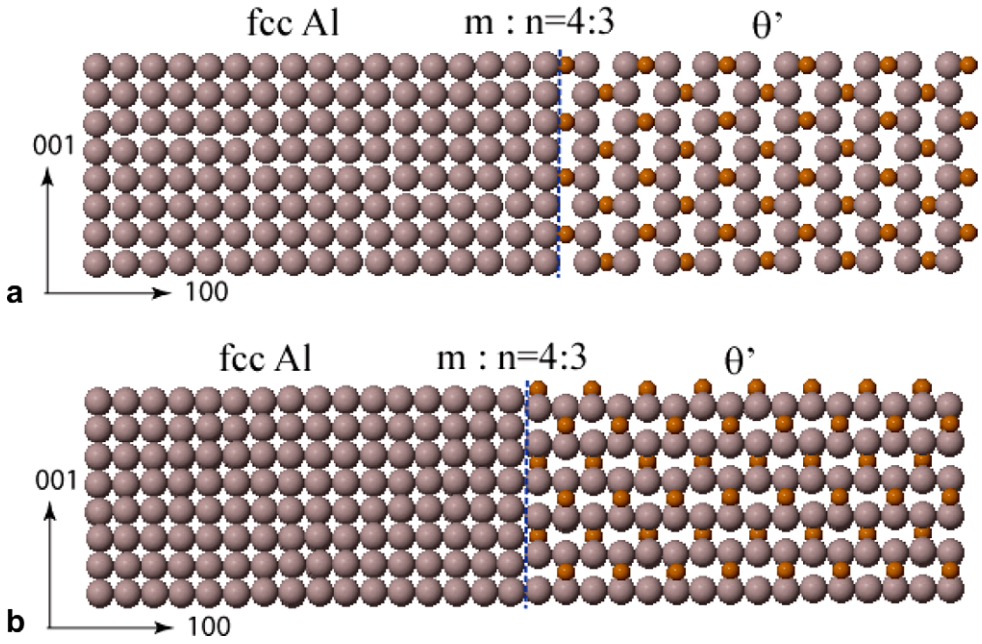

Fig. 5. Simulation cells for (a) the coherent and (b) the semicoherent interfacial energy calculations. The gray spheres denote Al atoms while the red spheres denote Cu atoms (For interpretation of the references to color in this figure legend, the reader is referred to the web version of this article.).

Table 4
Interface configuration *m*:*n* and stress-free strain

m	*n*	Stress-free strain
3	2	−0.0429
4	3	0.0767
5	3	−0.1386
7	5	0.0254
8	5	−0.1027

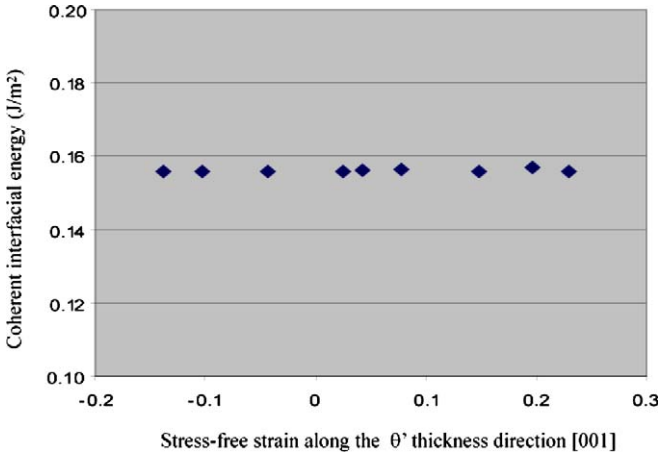

Fig. 6. Coherent interfacial energy versus stress-free strain.

interfacial energy for the interface with 3:2 match. This implies that the interface stresses do not significantly affect the semicoherent interfacial energy. Comparing the semicoherent interfacial energies with different interface configurations *m*:*n*, we found that the semicoherent interfacial energy is not particularly sensitive to the interface configurations, although it increases with an increase of stress-free strain.

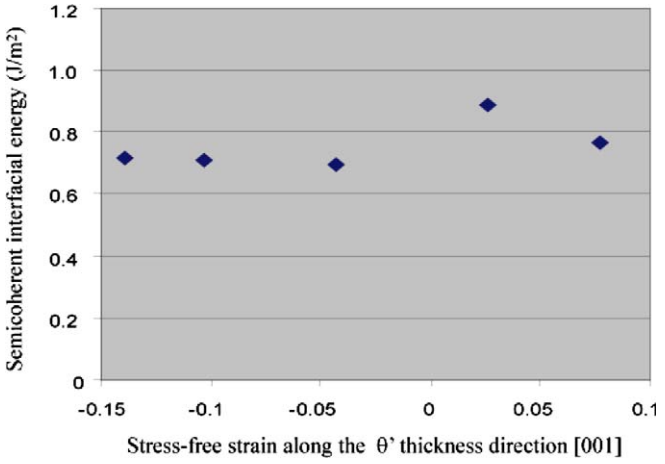

Fig. 7. Semicoherent interfacial energy versus stress-free strain.

4. Prediction of the critical nucleus size

4.1. Theoretical prediction of the critical nucleus size

Using the coherent and semicoherent interfacial energies obtained above, we predict the energetically favored shape and critical size of the θ' nucleus. Assuming that the semicoherent interfacial energy is isotropic, the total energy change due to the formation of a penny-shaped nucleus can be calculated as

$$\Delta G = V(\Delta G_V^{\text{chem}} + \Delta G^{\text{elas}}) + A_{\text{coh}}\gamma_{\text{coh}} + A_{\text{semi-coh}}\gamma_{\text{semi-coh}} \tag{17}$$

where V is the volume of the nucleus, A_{coh} and $A_{\text{semi-coh}}$ are the areas of coherent and semicoherent interface of the nucleus, respectively, γ_{coh} and $\gamma_{\text{semi-coh}}$ are the coherent and semicoherent interfacial energies, ΔG_V^{chem} is the chemical energy difference between the matrix and θ' and ΔG^{elas} is the elastic energy in an infinite matrix with a θ' precipitate. With the assumption of homogeneous and isotropic elasticity, for a penny-shaped nucleus with a radius R and an aspect ratio ($a = 2 * R/(ma_0)$, where a_0 is the lattice constant of fcc Al), ΔG^{elas} can be analytically calculated from the Eshelby's solution [27]:

$$\begin{aligned}\Delta G^{\text{elas}}/\mu = \Bigg[&(\varepsilon_{11}^{*\,2} + \varepsilon_{22}^{*\,2})\left(\frac{v}{1-v} - \frac{13}{32(1-v)}\frac{\pi}{a} + 1\right) \\ &+ \varepsilon_{33}^{*\,2}\frac{1}{4(1-v)}\frac{\pi}{a} + 2\varepsilon_{11}^{*}\varepsilon_{22}^{*}\left(\frac{v}{1-v} - \frac{16v-1}{32(1-v)}\frac{\pi}{a}\right) \\ &+ (2\varepsilon_{11}^{*}\varepsilon_{33}^{*} + 2\varepsilon_{22}^{*}\varepsilon_{33}^{*})\frac{2v+1}{8(1-v)}\frac{\pi}{a} \\ &+ (2\varepsilon_{23}^{*\,2} + \varepsilon_{31}^{*\,2})\frac{2-v}{4(1-v)}\frac{\pi}{a} + 2\varepsilon_{12}^{*\,2}\left(1 - \frac{7-8v}{16(1-v)}\frac{\pi}{a}\right)\Bigg]\end{aligned} \tag{18}$$

where ε_{ij}^{*} are components of the stress-free strain tensor associated with lattice mismatch, μ the shear modulus and v the Poisson ratio. For fcc Al, the elastic constants at room temperature are $C_{11} = 108$ GPa, $C_{12} = 62$ GPa and $C_{44} = 28.3$ GPa [25]. The elastic constants of θ' at 0 K are $C_{11} = 190$ GPa, $C_{12} = 80$ GPa and $C_{44} = 90$ GPa obtained from first-principals calculations [11]. We can see that the θ' precipitate is much stiffer than the matrix; thus the assumption of homogeneity is violated. In order to use Eqs. (17) and (18) to estimate the shape the size of critical nucleus, we assume effective elastic constants. In the calculations, the Poisson ratio $v = 0.345$ was taken from polycrystalline Al [22]. We changed the shear modulus from $\mu = 28.3$ to 90 GPa to examine the effect of elastic inhomogeneity on the shape the size of critical nucleus.

At finite temperatures, the contribution of vibration entropy to ΔG should be taken into account, which requires an accurate calculation of free energies and interfacial energies at different temperatures. In the present work, we focus on studying the critical size of θ' precipitates at 0 K. For the three interface configurations considered above, i.e., $m{:}n = 2{:}1.5$, 3:2 and 4:3, the total energy changes ΔG with respect to R have been calculated for the range of the shear modulus and plotted in Fig. 8. It can be seen that the nucleus with three fcc unit cells and two θ' unit cells match has the lowest critical nucleation energy barrier and also the smallest critical size. The nucleus with 2:1.5 match has a slightly higher nucleation barrier, and a much larger critical nucleus size. Compared to the nucleus with 3:2 match, the nucleus with 4:3 match has both a higher critical nucleation barrier and larger critical size. Therefore, the nucleus with 3:2 match is predicted

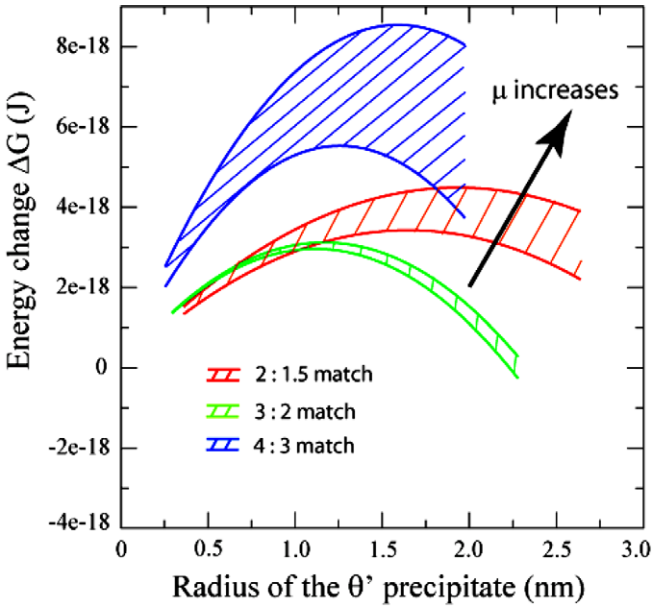

Fig. 8. Theoretical prediction of critical sizes for different semicoherent interface configurations ($m{:}n = 2{:}1.5$, 3:2 and 4:3). As the shear modulus μ increases, the critical sizes and nucleation barriers increase for the three different interface configurations.

to be the energetically and kinetically favored nucleus for θ' precipitation in Al–Cu alloys under the condition of homogeneous nucleation. Its critical size is about 2.4 nm, and critical nucleation energy barrier is about 3×10^{-18} J. In addition, we can see a common trend that the critical sizes and nucleation barriers increase as the shear modulus μ increases.

4.2. Atomistic simulations

As shown in the previous section, the theoretical prediction of critical nucleus size needs to assume isotropic and homogenous elasticity and an isotropic semicoherent interfacial energy. However, direct atomistic simulations can eliminate these assumptions and predict the critical nucleus size as well. To do so, the energy change must be calculated for different size θ' nuclei in an Al–1.7 at.% Cu solid solution. The simulations were performed on a $30a_0 \times 20a_0 \times 30a_0$ cell, where $a_0 = 0.405$ nm is the lattice constant of fcc Al. θ' precipitates with different sizes ($R = a_0$, $2a_0$,... and $6a_0$) have been artificially placed in the center of the simulation cell for each interface configuration ($m{:}n =$ 2:1.5, 3:2 and 4:3) while the overall average composition of Cu was held fixed. The static relaxation method is employed to minimize the energy of the system using periodic boundary conditions. The energy differences ΔG between a relaxed configuration with a θ' precipitate and the homogeneous alloy, as functions of nucleus size, are shown in Fig. 9. It can be seen that although the energy change depends on the Cu distribution in the matrix, especially when the nucleus is small, the critical nucleus size and nucleation barrier can

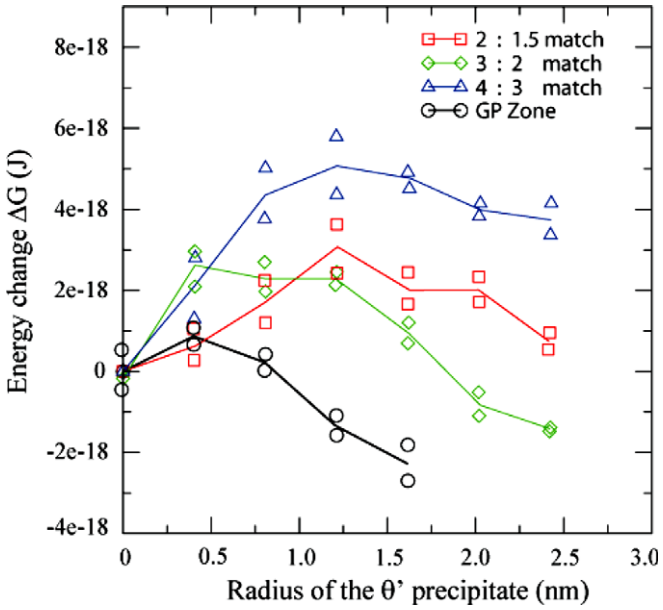

Fig. 9. Atomistic prediction of critical sizes. Data points represent individual simulation while the line traces the average of the points. The scattered symbols illustrate the variation of the energy calculated from different simulations with different Cu distributions in the matrix. The solid lines represent the average energy.

be identified. It is found that the nucleus with 3:2 match is the energetically and kinetically favored nucleus for θ' precipitation in Al–Cu alloys. The critical nucleus size is about 2.4 nm, and critical nucleation energy barrier is about 2.3×10^{-18} J. If we compare Fig. 8 with Fig. 9, it is clear that for all three interface configurations considered here the critical nucleus size and critical nucleation energy barrier predicted from atomistic simulations are all close to the lower bound predicted by theoretical calculation. The smaller values could be explained by the elastic relaxation and/or possible semicoherent interfacial energy anisotropy in the atomistic simulations. However, the atomistic simulations and theoretical calculation both predict consistent values of the critical nucleus sizes and the nucleation energy barriers for the three different interface configurations. The Guinier–Preston (GP) zone in Al–Cu alloys is a pure Cu layer on a (100) plane in an fcc Al–Cu solid solution. The energy changes due to the formation of a GP zone have also been calculated and are shown in Fig. 9. The predicted critical size of a GP zone is less than 0.8 nm, and the critical nucleation energy barrier is much smaller than that of θ' precipitates. Thus, as seen experimentally, a GP zone would form before a θ' precipitate.

Three-dimensional structures of the GP zone and θ' precipitates with different sizes and interface configurations $m{:}n = 2{:}1.5$, 3:2 and 4:3 have been examined. It is found that: a local contraction takes place around small Cu atoms; GP zones and θ' precipitates are stable structures; and their broad (001) interfaces are coherent. The relaxed atomic configurations on the (010) plane for the precipitates at their critical sizes are shown in Fig. 10. It can be seen that uniform contraction or expansion occurs along the thickness direction in the center region of the plate-like precipitates. Around the rim of the precipitate,

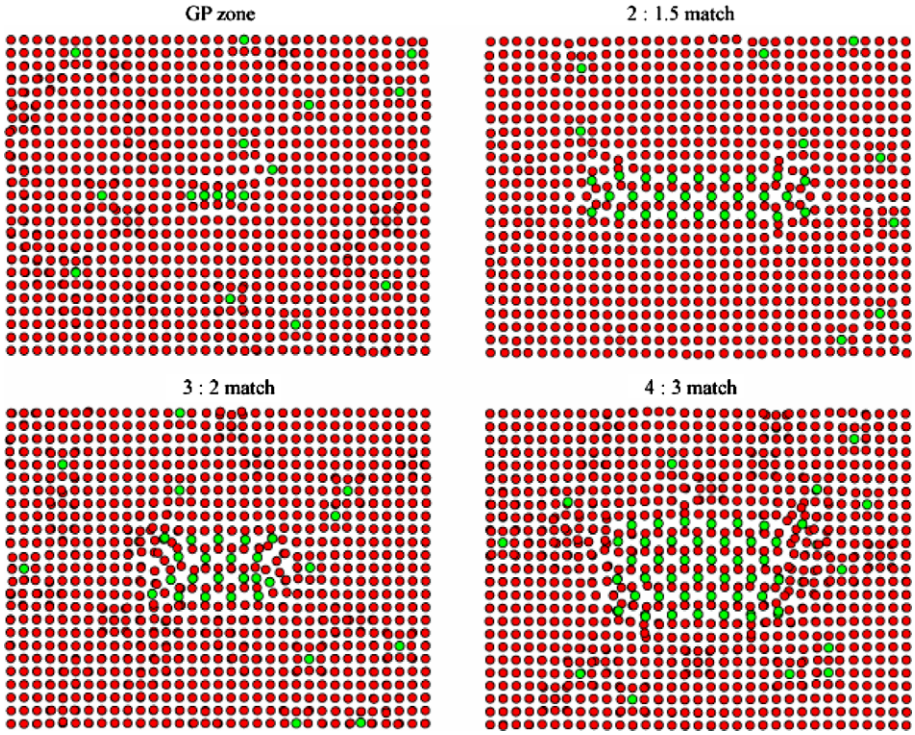

Fig. 10. Interface structures of θ' precipitates and a GP zone at their critical sizes.

the deformations in both the precipitate and the matrix are not uniform, and the interfaces are semicoherent.

5. Conclusion

We have developed MEAM potentials for Al–Cu alloys. The lattice constants and formation energies of θ' and θ phases, and the temperature dependence of the elastic constants of fcc Al and Cu predicted by these MEAM potentials are in good agreement with experimental data and first-principles calculations. Using these potentials, the coherent and semicoherent interfacial energies with different interface configurations have been calculated. It was found that semicoherent interfacial energies slightly depend on the interface configurations. The MEAM-calculated coherent interface energy is slightly smaller than that obtained from first-principles calculations, while for the semicoherent interface configuration with 3:2 match the semicoherent interfacial energy is slightly larger than that obtained from first-principles calculations. Both a theoretical method using the calculated interfacial energies and direct atomistic simulations predict that the nucleus with 3:2 match is the energetically favored shape. The critical nucleus size is about 1.6–2.4 nm and the energy barrier for the nucleation is about 2.3×10^{-18}–3.0×10^{-18} J.

Acknowledgements

The authors thank Richard G. Hoagland, H. Weiland, and J. Murray for valuable discussions. This work was supported at Los Alamos National Laboratory by the US Department of Energy under Contract W-7405-ENG-36, NSF under Grant number DMR-0205232 (L.Q.C.) and Alcoa (L.Q.C.).

References

[1] Doherty RD. In: Cahn RW, Hassen P, editors. Physical metallurgy. New York: Elsevier Science; 1996.
[2] Wolverton C, Ozolins V. Phys Rev Lett 2001;86:5518.
[3] Nakamura F, Furukawa F, Yanai M, Takamura J. Philos Mag 1986;A54:67.
[4] Matsabura E, Cohen JB. Acta Metall 1985;33:1945.
[5] Matsabura E, Cohen JB. Acta Metall 1985;33:1957.
[6] Wada M, Kita H, Mori T. Acta Metall 1985;33:1631.
[7] Ringer SP, Hono K, Sakurai T. Metall Mater Trans 1995;A26:2207.
[8] Boyd JD, Nicholson RB. Acta Metall 1971;19:1101.
[9] Boyd JD, Nicholson RB. Acta Metall 1971;19:1379.
[10] Aaronson HI, Laird C. In Ford Motor Co. Scientific Laboratory Report, 1967.
[11] Vaithyanathan V, Wolverton C, Chen LQ. Phys Rev Lett 2002;88:125503.
[12] Daw MS, Foiles SM, Baskes MI. Mater Sci Rep 1993;9:251.
[13] Daw MS, Baskes MI. Phys Rev Lett 1983;50:1285;
Phys Rev B 1984;29:6443.
[14] Baskes MI. Phys Rev Lett 1987;59:2666;
Phys Rev B 1992;46:2727.
[15] Baskes MI, Muralidharan K, Stan M, Valone SM, Cherne FJ. J Organomet Chem 2003;55:41.
[16] Baskes MI, Chen SP, Cherne FJ. Phys Rev B 2002;66:104107.
[17] Ravelo R, Baskes MI. Phys Rev Lett 1997;79:2482.
[18] Baskes MI, Angelo JE, Bisson CL. Model Simul Mater Sci Eng 1994;2:505.
[19] Baskes MI. Mater Chem Phys 1997;50:152.
[20] Rose JH, Smith JR, Guinea F, Ferrante J. Phys Rev B 1984;29:2963.
[21] Brandes EA, editor. Smithells metals reference book. London: Butterworths; 1983.
[22] Murray JL. Int Met Rev 1985;30:211.
[23] Jaffe JE, Kurtz RJ, Gutowski M. Computat Mater Sci 2000;18:199.
[24] Lu ZW, Wei SH, Zunger A. Phys Rev B 1990;41:2699.
[25] Ravelo R et al. Phys Rev B 1998;57:862.
[26] Simmons G, Wang H, editors. Single crystal elastic constants and calculated aggregate properties: a handbook. Cambridge: MIT Press; 1985.
[27] Mura T. Micromechanics of defects in solids. Dordrecht: Kluwer Academic; 1982.